

Synthesis and characterization of $\text{Fe}_3\text{O}_4@\text{SiO}_2@\text{PDA}@\text{Ag}$ core-shell nanoparticles and biological application on human lung cancer cell line and antibacterial strains

Snigdha Singh, Tanya Goel, Aarushi Singh, Heerak Chugh, Nayanika Chakraborty, Indrajit Roy, Manisha Tiwari & Ramesh Chandra

To cite this article: Snigdha Singh, Tanya Goel, Aarushi Singh, Heerak Chugh, Nayanika Chakraborty, Indrajit Roy, Manisha Tiwari & Ramesh Chandra (2024) Synthesis and characterization of $\text{Fe}_3\text{O}_4@\text{SiO}_2@\text{PDA}@\text{Ag}$ core-shell nanoparticles and biological application on human lung cancer cell line and antibacterial strains, *Artificial Cells, Nanomedicine, and Biotechnology*, 52:1, 46-58, DOI: [10.1080/21691401.2023.2295534](https://doi.org/10.1080/21691401.2023.2295534)

To link to this article: <https://doi.org/10.1080/21691401.2023.2295534>



© 2023 The Author(s). Published by Informa UK Limited, trading as Taylor & Francis Group



Published online: 29 Dec 2023.



Submit your article to this journal [↗](#)



Article views: 382





View related articles [↗](#)



View Crossmark data [↗](#)

Synthesis and characterization of $\text{Fe}_3\text{O}_4@\text{SiO}_2@\text{PDA}@Ag$ core-shell nanoparticles and biological application on human lung cancer cell line and antibacterial strains

Snigdha Singh^a , Tanya Goel^{a,b,t}, Aarushi Singh^{a,c,t}, Heerak Chugh^a, Nayanika Chakraborty^a, Indrajit Roy^a, Manisha Tiwari^b and Ramesh Chandra^{a,b} 

^aDepartment of Chemistry, University of Delhi, Delhi, India; ^bDr. B. R. Ambedkar Center for Biomedical Research, University of Delhi, Delhi, India; ^cMax Planck Institute for Multidisciplinary Sciences, Göttingen, Germany

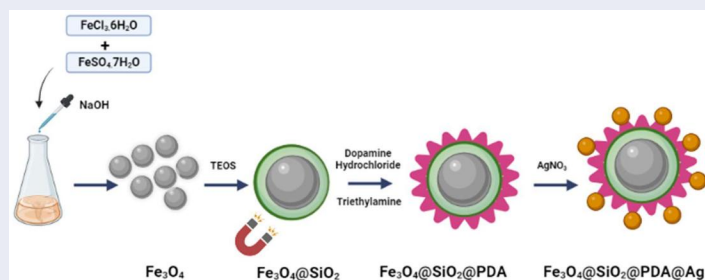
ABSTRACT

Novel magnetic and metallic nanoparticles garner much attention of researchers due to their biological, chemical and catalytic properties in many chemical reactions. In this study, we have successfully prepared a core-shell $\text{Fe}_3\text{O}_4@\text{SiO}_2@\text{PDA}$ nanocomposite wrapped with Ag using a simple synthesis method, characterised and tested on small cell lung cancer and antibacterial strains. Incorporating Ag in $\text{Fe}_3\text{O}_4@\text{SiO}_2@\text{PDA}$ provides promising advantages in biomedical applications. The magnetic Fe_3O_4 nanoparticles were coated with SiO_2 to obtain negatively charged surface which is then coated with polydopamine (PDA). Then silver nanoparticles were assembled on $\text{Fe}_3\text{O}_4@\text{SiO}_2@\text{PDA}$ surface, which results in the formation core-shell nanocomposite. The synthesised nanocomposite were characterized using SEM-EDAX, dynamic light scattering, XRD, FT-IR and TEM. In this work, we report the anticancer activity of silver nanoparticles against H1299 lung cancer cell line using MTT assay. The cytotoxicity data revealed that the IC_{50} of $\text{Fe}_3\text{O}_4@\text{SiO}_2@\text{PDA}@Ag$ against H1299 lung cancer nanocomposites cells was 21.52 $\mu\text{g}/\text{mL}$. Furthermore, the biological data of nanocomposites against Gram-negative '*Pseudomonas aeruginosa*' and Gram-positive '*Staphylococcus aureus*' were carried out. The range of minimum inhibitory concentration was found to be 115 $\mu\text{g}/\text{mL}$ where gentamicin was used as a standard drug. The synthesized AgNPs proves its supremacy as an efficient biomedical agent and AgNPs may act as potential beneficial molecule in lung cancer chemoprevention and antibacterial strains.

KEY MESSAGES

1. In the present study, we have successfully prepared a core-shell $\text{Fe}_3\text{O}_4@\text{SiO}_2@\text{PDA}@Ag$ nanocomposite.
2. We have investigated the dose-dependent cellular toxicity of silver nanocomposite in the nonsmall cell lung cancer cell line H1299 using MTT assay.
3. Also, we have evaluated the mode of cell death using apoptosis.
4. We have also evaluated the bioactivity of AgNPs on both Gram-positive and Gram-negative bacterial cells with highly efficient antibacterial potency.

GRAPHICAL ABSTRACT



ARTICLE HISTORY

Received 24 April 2023
Revised 30 November 2023
Accepted 6 December 2023

KEYWORDS

lung cancer; silver nanocomposite; polydopamine; biomedical application; antibacterial strains; silver nanoparticles (AgNPs)

1. Introduction

Lung cancer is dominant and second most commonly diagnosed cancer among men and women which is largely

widespread around the globe. It has a high morbidity and mortality rates worldwide, causing 1.8 million deaths [1]. However, the nanoparticles have proven as an effective tools

CONTACT Ramesh Chandra  acbrdu@hotmail.com  Department of Chemistry, University of Delhi, Delhi 110007, India

[†]These authors contributed equally to this work.

© 2023 The Author(s). Published by Informa UK Limited, trading as Taylor & Francis Group
This is an Open Access article distributed under the terms of the Creative Commons Attribution-NonCommercial License (<http://creativecommons.org/licenses/by-nc/4.0/>), which permits unrestricted non-commercial use, distribution, and reproduction in any medium, provided the original work is properly cited. The terms on which this article has been published allow the posting of the Accepted Manuscript in a repository by the author(s) or with their consent.

from its diagnosis to cancer therapy [2]. The size of synthetic nanoparticle derived from polymers, metals etc. having a diameter of <100 nm are particularly useful as size is similar to most of the biological structures and molecules. Hence, they confer functional properties for both *in vitro* and *in vivo* cancer research [3]. Silver NPs (AgNPs) show significant features like high catalytic activity, chemical stability, easy fabrication, good conductivity and potential therapeutical application such as antibacterial [4], anticancer [5,6], anti-inflammatory activities [7,8], nanoelectronic devices, water purification, and environmental pollution control [9,10]. Despite from other metal nanoparticles, silver nanoparticles are nontoxic at lower dosage for a human body [11,12]. The high surface to volume ratios of silver nanoparticles have high reactivity and hence provide its usage in biomedical applications. Recently, core shell AgNPs has been studied for effective gene delivery and it showed that it can completely condensate DNA and protect it from degradation [13]. Also hybrid $\text{Fe}_3\text{O}_4@$ AgNPs were synthesised *via* green route and demonstrated selective cytotoxicity against tumour cell line [14]. Silver nanoparticles (AgNPs) have now been recognised as significant class of nanomaterials for various biomedical applications and more attention are focused on AgNPs because they have risen up as promising therapeutic molecule in cancer treatment [15]. AgNPs have exhibited potential cytotoxicity against various cancer cell lines like lung cancer A549 [16–18], Hela cells [19], breast cancer MCF-7 cells [20–22] and so on. Furthermore, as we all are aware that bacterial infections are major threat to public health globally. Several nanocomposites based on Au [23], Ag [24,25], Cu [26,27] and ZnO [28] have been used as antibacterial agents [29]. As we know, various processes have now been established to synthesise highly dispersed AgNPs using solution based methods, therefore in order to address this challenge, increasing efforts has been aimed towards AgNPs introduction on solid supports (polymers, metal oxides) using different nanostructures like spheres, mesoporous silica to generate composite catalysts, which could be the best approach to avoid aggregation of small-sized AgNPs without affecting properties [30,31].

A new trend in field of material sciences is coating of materials and modifying their surface which can provide novel surface functionalities and properties [32]. Recently, three layered core-shell nanocomposites have gained much attention in cancer application. Among the other preferred carrier materials, silica coated with Fe_3O_4 magnetic carrier have emerged as a powerful catalytic support as they have excellent thermal stability, low toxicity, ease of synthesis, effortless separation from the reaction through external magnetic sources [33]. The SiO_2 core have some advantages like ease in controlling particle size, high colloidal stability and has potential application in drug delivery and biosensors [34,35]. However, the surface properties of silica nanoparticles have been found tuneable for various purposes like multi-functionalization, drug loading, drug release and delivery [36]. Usually, a nanomaterial using Fe_3O_4 core and SiO_2 shell has a good magnetic response and chemically modifiable surface. Polydopamine (PDA) has been

extensively used as a versatile functionalization tool since 2007, having been inspired by adhesive nature of amines and catechols in mussel adhesive proteins [37]. These PDA could self-polymerize and form PDA layers which can be subsequently applied to variety of substrates to improve biocompatibility and to tolerate other bio-functionalization [38,39]. PDA can readily be deposited under slightly basic conditions by dopamine polymerization, to form a biocompatible layer that will stick to range of material surfaces [40,41]. The metallic nanoparticles like Ag, Au Pd in combination with other metal oxides like (SiO_2 , TiO_2), polymer matrices like polyaniline, PDA, pyrrolidone, polypyrrole have been exponentially explored due to high conductivity, thermal stability and redox potential nanocomposites [42].

Recently, Zhang et al. [43] reported the green synthesis of AgNPs decorated on $\text{Fe}_3\text{O}_4@$ PDA as effective antimicrobial agents. Wang et al. [44] have synthesised PDA coated magnetic nanocellulose AgNP for inactivation of *E. coli* bacteria in waste water. Nikmah et al. [45] have reported the synthesis of $\text{Fe}_3\text{O}_4@$ $\text{SiO}_2@$ Ag nanocomposites and promising antibacterial activity using agar diffusion method. Baoliang et al. [46] have reported a composite of $\text{Fe}_3\text{O}_4@$ $\text{SiO}_2@$ Ag and their application in Surface enhanced Raman Scattering. Similarly, novel cube like $\text{Fe}_3\text{O}_4@$ $\text{SiO}_2@$ Au@Ag magnetic nanocomposites have been reported as efficient SERS substrate for pesticide detection [47]. Here, $\text{Fe}_3\text{O}_4@$ $\text{SiO}_2@$ PDA core has been used as the support for Ag nanoparticles. In order to improve the biocompatibility of the nanopatform, for the first time we report the fabrication and characterization of the synthesised ' $\text{Fe}_3\text{O}_4@$ $\text{SiO}_2@$ PDA@Ag' nanocomposites where SiO_2 nanoparticles were synthesised by hydrolysis of TEOS followed by thermal decomposition and its used as core for synthesis for core-shell nanoparticles. Various studies reveal that Ag nanocomposites decorated with ferrite-silica core have the potential to destroy cancer cells without affecting the normal cells. Therefore, in the present study, we have investigated the dose-dependent cellular toxicity of silver nanocomposite in the non-small cell lung cancer cell line H1299 by the MTT. Also we have evaluated the mode of cell death using apoptosis. We have also evaluated the bio-activity of AgNPs on both Gram-positive and Gram-negative bacterial cells with highly efficient antibacterial potency and can be exploited as drugs next door in potential healthcare settings.

2. Experimental

2.1. Materials and reagents

$\text{FeCl}_3 \cdot 6\text{H}_2\text{O}$ was purchased from Central Drug House Pvt. Ltd, $\text{FeSO}_4 \cdot 7\text{H}_2\text{O}$, tetraethyl orthosilicate (TEOS) from Sigma Aldrich. The ethyl alcohol ($\text{C}_2\text{H}_5\text{OH}$, 95%), and aqueous ammonia (25 wt%) were supplied by SRL Co., Ltd. All chemical reagents were directly used without further purification. MTT dye was purchased from Sigma Aldrich. Double deionised water was used throughout the study. All reagents were used without purification.

2.2. Synthesis of ferrite (Fe_3O_4) nanoparticles

Initially, $\text{FeCl}_3 \cdot 6\text{H}_2\text{O}$, 6.0 g and $\text{FeSO}_4 \cdot 7\text{H}_2\text{O}$, 4.2 g were dissolved in 250 ml of deionised water and were allowed to stir at 50 °C until appearance of yellow-orange solution. After, we added 25% ammonium hydroxide dropwise to slowly adjust the pH to 10 and then the mixture was allowed to stir for another 1 h at 50 °C [48]. The ferrite nanoparticles were precipitated as a black material which was separated by an external magnet and washed several times with water and ethanol. This was dried overnight in oven at 50 °C to obtain the nanoparticles.

2.3. Synthesis of $\text{Fe}_3\text{O}_4@SiO_2$

The SiO_2 coating over ferrite nanoparticles was done using sol-gel approach. A suspension of 0.5 g of ferrite nanoparticles and 0.1 M HCl (2.2 ml) was prepared in water (50 ml) and ethanol (200 ml) mixture under sonication for 1 h at RT. After, 25 % NH_4OH (5 ml) was added to the mixture followed by dropwise addition of TEOS (1 ml) and resulting mixture was stirred at 50 °C for 6 h. The resulted silica coated magnetic nano particles $\text{Fe}_3\text{O}_4@SiO_2$ were separated magnetically and washed with ethanol and water several times and then dried in oven at 40 °C.

2.4. Synthesis of $\text{Fe}_3\text{O}_4@SiO_2@PDA$

The $\text{Fe}_3\text{O}_4@SiO_2$ nanoparticles (0.18 g) were dispersed *via* sonication into ethanol (100 ml) for half hour. Then dopamine hydrochloride (100 mg) and triethylamine (74 μL) were added to the reaction mixture. The mixture was then stirred at 50 °C for 24 h and then nanoparticles were purified by three wash cycles of centrifugation/redispersion in ethanol [32,49].

2.5. Synthesis of $\text{Fe}_3\text{O}_4@SiO_2@PDA@Ag$

$\text{Fe}_3\text{O}_4@SiO_2@PDA$ nanospheres (100 mg) were dispersed in 100 ml water. In another beaker, dissolve 50 mg silver nitrate in 100 ml water. Mix the above two solutions and allowed to stir for 24 h. The mixture was washed with water and ethanol several times and then dried at 50 °C

3. Characterization of synthesised $\text{Fe}_3\text{O}_4@SiO_2@PDA@Ag$

3.1. Electron microscopy

To determine the size and morphology of synthesised nanocomposite, $\text{Fe}_3\text{O}_4@SiO_2@PDA@Ag$ was subjected to transmission electron microscopy using TEM (TALOSTEM from Thermo Scientific). For TEM analysis, carbon-coated Cu grids were used, and the sample was deposited on them using the drop-casting method. Image J software was used to calculate the average size of nanoparticles.

0.5 mg of nanocomposite was diluted with 70% ethanol (1 ml), sonicated for 30 min before placing onto carbon coated copper grid.

The $\text{Fe}_3\text{O}_4@SiO_2@PDA@Ag$ was subjected to FESEM-EDAX using Zeiss GeminiSEM 500 thermal field emission type microscope.

3.2. Particle size and zeta potential

Nanoparticle samples were dispersed, sonicated for 5 min in milliQ water and 1 ml of this was taken in quartz cuvette before analysis. The particle size was measured using dynamic light scattering (DLS), Nanoplus particle size analyser from Particulate Systems and surface charge measurement of nanocomposite were measured by Zetasizer Nano-ZS (Malvern Instruments, UK). All measurements were carried out in triplicate ($n = 3$).

3.3. Fourier-transforms infra-red (FT-IR) spectroscopy

FTIR was performed using Shimadzu II FT-IR Spectrometer. In brief, spectrum for physical mixture of Fe_3O_4 , $\text{Fe}_3\text{O}_4@SiO_2$ and $\text{Fe}_3\text{O}_4@SiO_2@PDA$ as well as $\text{Fe}_3\text{O}_4@SiO_2@PDA@Ag$ was recorded.

3.4. Powder X-ray diffraction pattern (PXRD)

The polymorphic state of the drug in lipid matrix was confirmed using Rigaku Ultima IV X-ray Diffractometer. The Ni-filtered, Cu K α -radiation, voltage of 40 Kv and current of 40 mA was used. The scanning rate was 1°/min over 10 °–50° diffraction angle (2θ) range. The crystal lattice of $\text{Fe}_3\text{O}_4@SiO_2@PDA@Ag$ was accounted.

3.5. Stability data

The stability analysis of $\text{Fe}_3\text{O}_4@SiO_2@PDA@Ag$ nanocomposites was performed using DLS measurements at different time intervals. The suspension of AgNPs were kept at 4 °C and size measurements at different time intervals was observed using DLS at 1, 7, 14, and 21 days. Also, we have prepared the suspension of AgNPs in different PBS buffers (neutral, acidic and basic) and size was recorded [50,51].

4. Cellular experiments

Human lung adenocarcinoma H1299 cancer cells were purchased from the Cell Bank of Type Culture Collection of ACBR and cultured in DMEM supplemented with 10% foetal bovine serum and 1% penicillin/streptomycin in a cell culture incubator maintained under a 5% CO_2 atmosphere at 37 °C.

Gram positive '*Staphylococcus aureus*' (*S. aureus*, MTCC 741) and Gram negative '*Pseudomonas aeruginosa*' (*P. aeruginosa*) were the microbes used in this study. Both *S. aureus* and *P. aeruginosa* were grown and cultured in Brain Heart Infusion (BHI) media procured from HiMedia at 37 °C and 180 rpm for 12 h. Furthermore, pure colony of these bacteria were collected with a sterile inoculating loop from agar plate and sub cultured in BHI broth and stored at 4 °C for future experimental purpose.

4.1. MTT assay

H1299 lung adenocarcinoma cell line was cultured in DMEM supplemented with 10% foetal bovine serum (FBS) and 1% antibiotics penicillin and streptomycin (100 µg/mL). Cells were maintained in humidified incubator at 5% CO₂ and 37 °C. Cells were passaged and harvested at ~80% confluency; they were seeded in 96 well plates at a cellular density of 7×10^3 cells per well. The seeded cells were grown overnight and treated with various concentrations of Fe₃O₄@SiO₂@PDA and Fe₃O₄@SiO₂@PDA@Ag nanocomposites in triplicates. A 2 mg/mL stock solution of Fe₃O₄@SiO₂@PDA and Fe₃O₄@SiO₂@PDA@Ag was prepared in MilliQ water and sonicated to achieve a homogenised solution. Carefully calculated amount of the nanocomposite was added to the 96 well plates for the following final concentrations- 5, 10, 20, 40, 60, 80, 100 µg/mL. The plates were then incubated at 37 °C, 5% CO₂ humidified incubator for 48 h. Post-incubation, the effect of Fe₃O₄@SiO₂@PDA and Fe₃O₄@SiO₂@PDA@Ag nanocomposite was evaluated using a freshly prepared Methylthiazolyldiphenyl-tetrazolium bromide (MTT) solution at a final concentration of 0.5 mg/mL each well. Next, 100 µL of DMSO was added to each well to dissolve the formazan crystals and reading was taken using a multiplate reader at 570 nm and reference at 630 nm.

$$\% \text{ Viability} = \frac{\text{Average reading at 570nm/}}{\text{Average reading of control at 570 nm}} \times 100$$

4.2. Apoptosis

The mode of cell death upon treatment with Fe₃O₄@SiO₂@PDA@Ag on H1299 cancer cell line was determined using Flow cytometer. The Annexin-FITC Apoptosis Detection Kit was used and the protocol was followed as per the manufacturer's protocol. In brief, H1299 cells were seeded separately in six-well cell culture with a total concentration of about 1×10^5 cells per well. Cells were grown for 24 h in DMEM medium containing 10% FBS prior to all experiments. The dosing solution was prepared in MilliQ the concentration close to IC₅₀ of Fe₃O₄@SiO₂@PDA@Ag was added to the well. Sample were incubated with cultured H1299 cells for 48 h. After predetermined incubation period, the treated cells were extensively rinsed with ice-cold PBS and harvested with Trypsin-EDTA, followed by centrifugation and washing with ice-cold PBS twice and incubated with Annexin/PI dye for 30 min. Then the analyses of the samples were performed on a flow cytometer at FL1 (FITC) and FL2 (PI) channels using BD FACS CALIBUR™. And data was further analysed using Cell Quest pro software.

4.3. Minimum inhibitory concentration (MIC)

MIC test is widely used in clinical microbiology as it provides the lowest concentration of the test antimicrobial agent required to inhibit the visible growth of the microorganism. In a 96-well sterile microtitration plate (Corning), we performed this microbroth dilution procedure with escalating dosages of the as-synthesised Fe₃O₄@SiO₂@PDA@Ag

nanocomposites. The final volume of 200 µL was achieved with 10 µL of mid-log phase bacterial inoculum and BHI broth with the desired nanoparticle concentration. Wells with only media and *S.aureus* or *P.aeruginosa* served as growth controls. The 96-well microtitration plates after inoculation was subjected to well-mixing and incubated in incubator shaker at 180 rpm and 37 °C for 16–18 h. The growth of the treated cells was monitored by measuring the absorbance at 600 nm in the TECAN Infinite M200 Pro, micro-plate reader.

4.3.1. SEM analysis of bacterial cell rupture on *P. Aeruginosa* cells

The structural changes in the bacterial morphology induced by as-synthesised Fe₃O₄@SiO₂@PDA@Ag nanocomposites were examined by Scanning Electron Microscopy. *Pseudomonas aeruginosa* was grown overnight at 37 °C under aerobic conditions. Then, 10^6 CFU/mL of the fresh cultures was used to carry out subsequent experiments. The bacterial suspensions were centrifuged at 4000 rpm for 10 min to separate bacterial pellets. The aqueous dispersion of nanoparticles (at MIC value) was incubated with freshly prepared culture of *P. aeruginosa*. The pellet appeared was thoroughly washed with 1X PBS solution (3 × 1 ml). After centrifugation, each bacterial pellet was fixed with 4% paraformaldehyde solution, and the pellet was kept at 4 °C overnight. After centrifugation, again the washing of each pellet was done with 1 × PBS (3 × 1 ml). Ultimately, serial dehydration of bacterial cells was carried out by washing with increasing concentrations of ethanol (10%, 20%, 40%, 60%, 80% and 100%). The pellet was dried and deposited on SEM stub for analysis.

4.4. In vitro Haemolysis assay

Haemolysis assay was done to ascertain the lytic interactions of as synthesised nanocomposites with the mammalian membrane. The whole blood sample was washed with 1 × PBS solution (pH = 7.4) and resuspended in PBS solution. 100 µL of diluted RBC suspension in 1 × PBS solution was exposed to various 100 µL of the nanoparticle suspension at concentration of 100, 250, 350, 450, 550 and 650 µg/mL (test group), PBS (positive group), and 1% TritonX-100 (negative group). After incubation at 37 °C for 1 h and centrifugation for 5 min at 800 g, the supernatant of all samples was transferred to a 96-well plate and the absorbance was measured by a microplate reader (BioTek 800 TS absorbance reader) at 405 nm. The percent haemolysis was expressed by the following formula and plotted as a function of percent haemolysis with concentration (µg/mL):

$$\% \text{ Haemolysis} = \frac{\text{OD (test)} - \text{OD (negative)}}{\text{OD (positive)} - \text{OD (negative)}} \times 100$$

5. Result and discussion

5.1. Characterization of synthesised Fe₃O₄@SiO₂@PDA@Ag

5.1.1. Electron microscopy

The TEM images suggested that particles were roughly spherical in shape as show in the figure below at 50 nm scale with

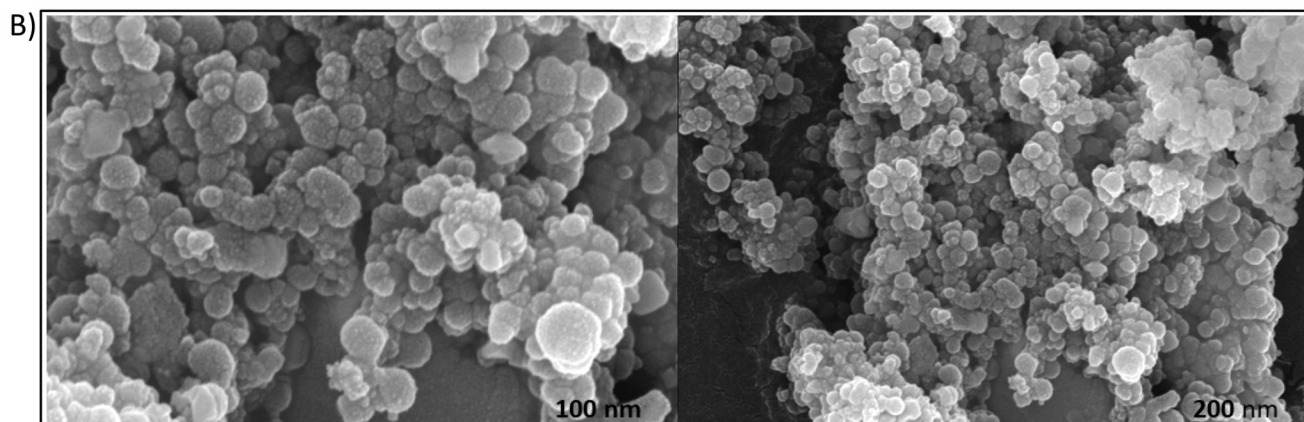
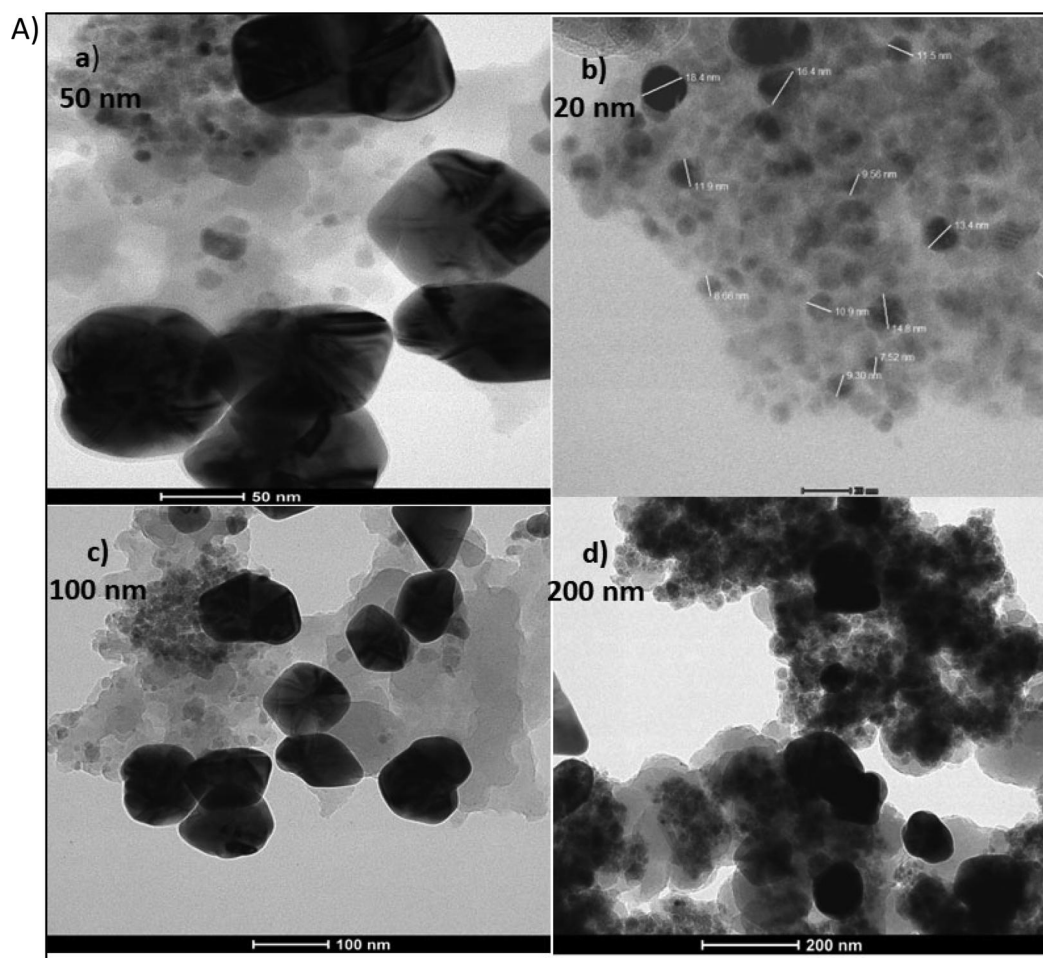


Figure 1. (a) TEM image of synthesised $\text{Fe}_3\text{O}_4@\text{SiO}_2@\text{PDA}@\text{Ag}$ nanocomposite. (a) 50 nm (b) 20 nm (c) 100 nm (d) 200 nm. (b) Fe-SEM image of synthesised $\text{Fe}_3\text{O}_4@\text{SiO}_2@\text{PDA}@\text{Ag}$ nanocomposite (a)100 nm (b) 200 nm (c) Elemental mapping image of synthesised $\text{Fe}_3\text{O}_4@\text{SiO}_2@\text{PDA}@\text{Ag}$ nanocomposite.

the size ranging from 10 to 30 nm (Figure 1). However, TEM image at 100 nm suggested that the nanocomposites are present in chain-like confirmation.

5.1.2. DLS and zeta potential

The formation of $\text{Fe}_3\text{O}_4@\text{SiO}_2@\text{PDA}@\text{Ag}$ was established by DLS study and the results revealed the hydrodynamic size of

the nanostructures was found to be ~ 139.1 nm at 25°C in water as solvent with polydispersity index of 0.237 (Figure 2). This could be due to the aggregation of the nanostructures in water. However, the average size difference in TEM and DLS could be due to the hydrodynamic diameter with swollen nanostructures in DLS [52,53]. The low zeta potential value of 5.02 mV indicates that nanostructures could agglomerate. (Figure 3).

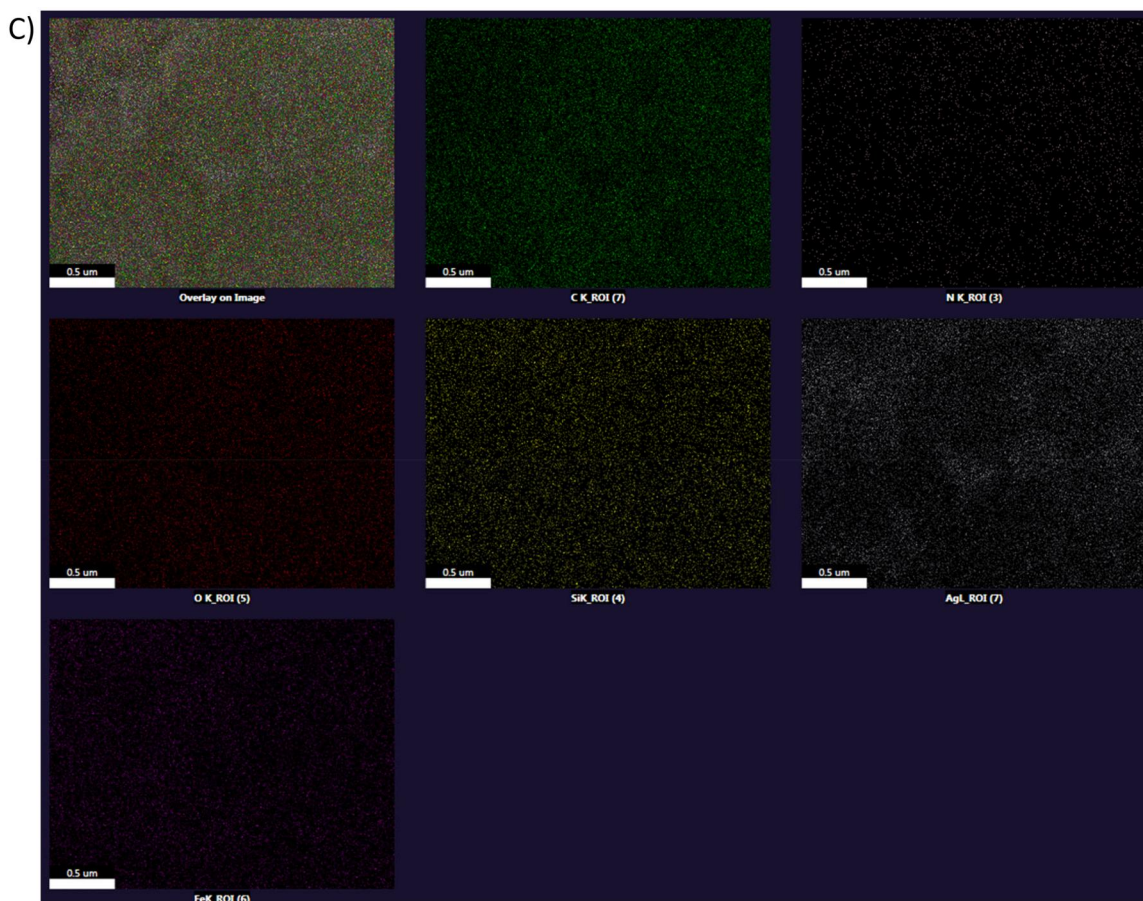


Figure 1. Continued.

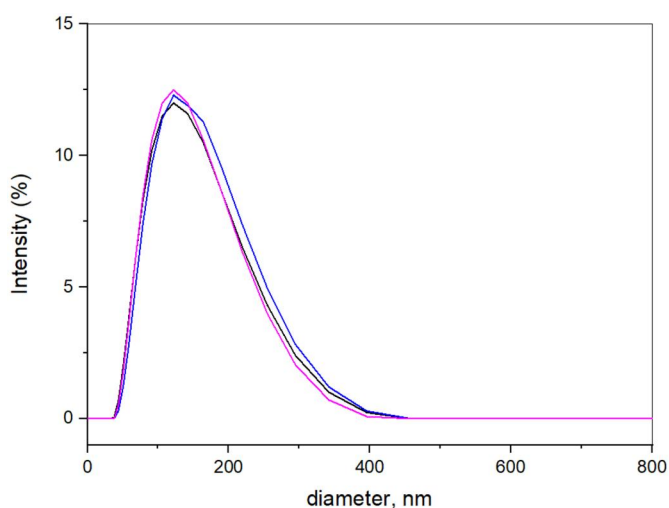


Figure 2. DLS of synthesised $\text{Fe}_3\text{O}_4@SiO_2@PDA@Ag$ (medium: Water; size, d : 139.1 nm).

5.1.3. FTIR spectra

FT-IR was used to study the successful immobilization of various functionalities at each step of nanocomposite preparation. The stretching frequency of Fe_3O_4 , $\text{Fe}_3\text{O}_4@SiO_2$, $\text{Fe}_3\text{O}_4@SiO_2@PDA$ as well as $\text{Fe}_3\text{O}_4@SiO_2@PDA@Ag$ have been recorded. The peak at 565 cm^{-1} is attributed to Fe–O vibration of the bulk Fe_3O_4 . The immobilization of the silane on the magnetic nanoparticle surface was confirmed

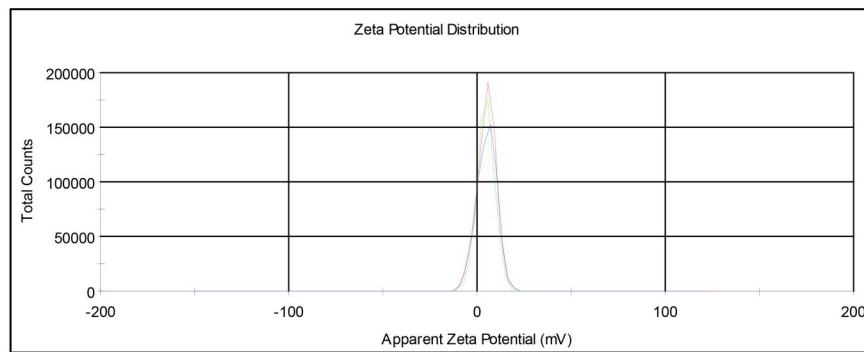
by the appearance of peaks at 455 cm^{-1} corresponding to Si–O–Si bending modes and peak at 1083 cm^{-1} corresponding to Si–O bending. However, the peak at 3385 cm^{-1} is due to O–H stretching vibrations of PDA and the peak displayed at 2372 cm^{-1} corresponds to C–H stretching vibrations. The appearance of peak at 1662 cm^{-1} is attributed to N–H group and the peaks at 1088 is associated with C–N stretching [53]. Hence, FT-IR spectra postulated that Fe_3O_4 , SiO_2 and PDA persisted its characteristics in the lipid matrix (Figure 4).

5.1.4. Powder X-ray diffraction (PXRD) pattern

In order to determine the chemical composition of the so-formed nanocomposites, XRD analysis of $\text{Fe}_3\text{O}_4@SiO_2@PDA@Ag$ was carried out. The peaks at 30.32° , 35.58° , 46.19° , 57.33° , 62.86° indicates the presence of magnetite nanoparticles. The position and relative intensities of all the peaks in the XRD pattern of $\text{Fe}_3\text{O}_4@SiO_2@PDA@Ag$ nanocomposite displayed the peaks at 38.11° , 43.25° , 62.86° , 77.46° that correspond to 111, 200, 220 and 311 planes of Silver nanoparticles [54] (Figure 5).

5.1.5. Elemental analysis

The EDX analysis of $\text{Fe}_3\text{O}_4@SiO_2@PDA@Ag$ nanocomposite displayed the presence of carbon, nitrogen, oxygen, silicon, silver and Iron in 6.71 wt %, 1.92 wt %, 32.36 wt %, 13.49 wt %, 11.15 wt % and 34.38 wt %, respectively (Figure 6).



Nanocomposite	Avg. Zeta Potential (mV)	Temp (°C)	Poly Dispersity Index (PDI)	Diameter, d (nm)	Solvent
Fe ₃ O ₄ @SiO ₂ @PDA@Ag	5.02	25	0.237	139.1	Water

Figure 3. Zeta potential distribution image of synthesised Fe₃O₄@SiO₂@PDA@Ag.

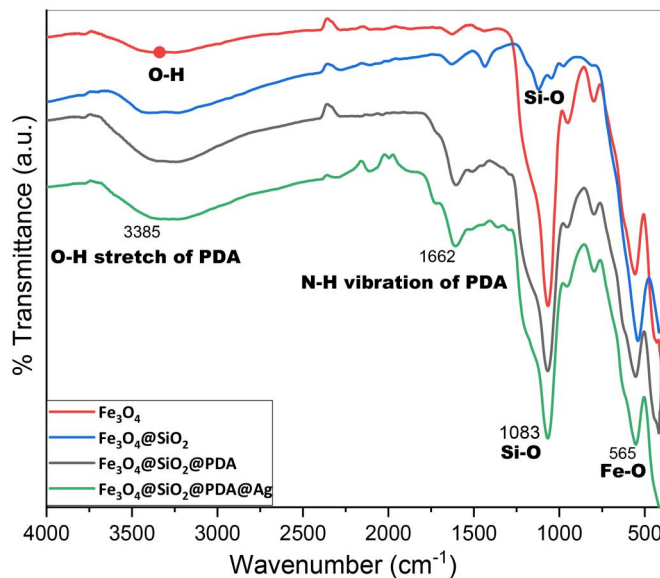


Figure 4. FT-IR of (a) Fe₃O₄, (b) Fe₃O₄@SiO₂, (c) Fe₃O₄@SiO₂@PDA, and (d) Fe₃O₄@SiO₂@PDA@Ag nanocomposite.

5.2. Stability data of the Fe₃O₄@SiO₂@PDA@Ag nanocomposite

The stability analysis of AgNPs was performed using DLS measurements at different time intervals. The suspension of AgNPs in water were made and kept at 4 °C and size was measured using DLS at 1, 7, 14, 21 days' time intervals. The size of AgNPs in water was found in the range of 120–150 nm. Also, size at different pH was measured and found to be in range of 130–300 nm in pbs and basic buffer, but in acidic buffer size increased to 500 nm after 14 days.

It can be concluded that particles have high stability despite pH and long storage (Figure 7).

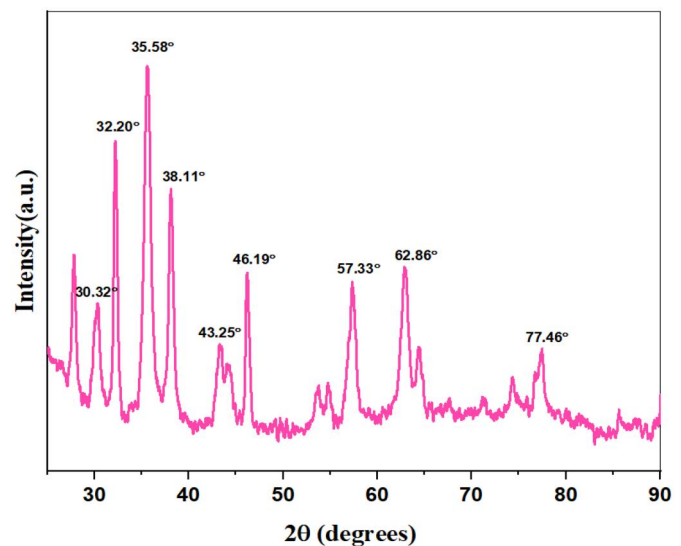


Figure 5. XRD of Fe₃O₄@SiO₂@PDA@Ag nanocomposite.

5.3. Biological analysis

5.3.1. Evaluation of cytotoxic effect of nanoparticles using MTT assay

MTT assay is among the few preliminary assays to assess the effectiveness or toxicity of small molecules, biomaterials etc. on cultured cells. MTT (3-(4,5-dimethylthiazol-2-yl)-2,5-diphenyltetrazolium bromide) is a yellow-coloured water-soluble dye that gives purple crystals on its reduction concept on which MTT assay is based upon. In a live cell, cellular respiration produces NADPH which reduces the yellow-coloured dye to purple formazan crystals after incubation; the amount of crystals formed or the amount of colour is directly proportional to levels of NADPH which in turn is proportional to cell viability. The formazan crystals are solubilised in DMSO and measured spectrophotometrically.

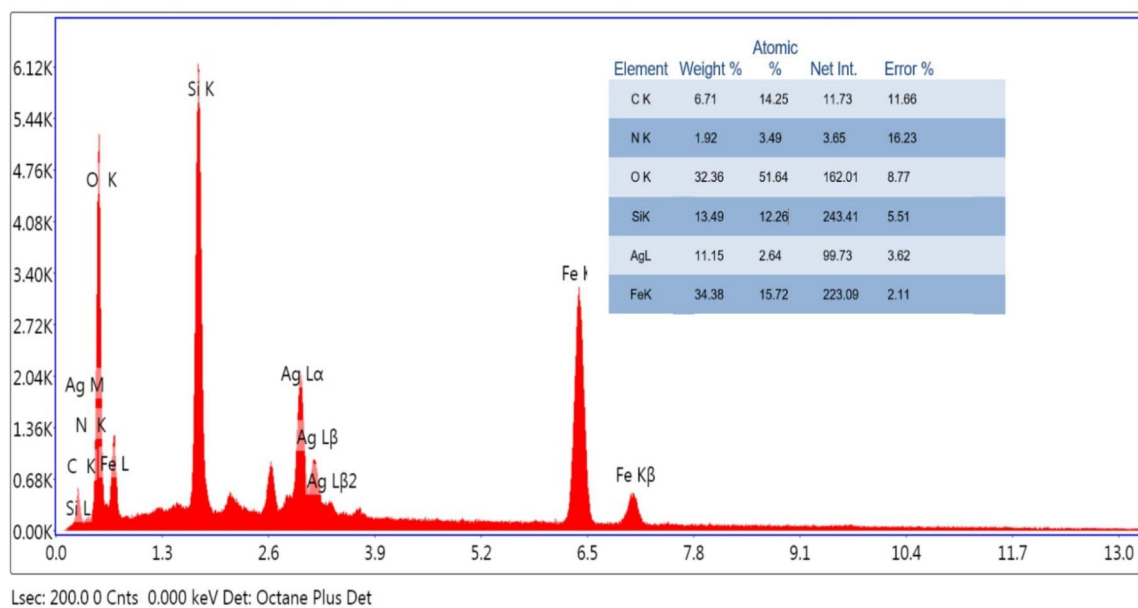


Figure 6. EDAX of $\text{Fe}_3\text{O}_4@\text{SiO}_2@\text{PDA}@\text{Ag}$ nanocomposite.

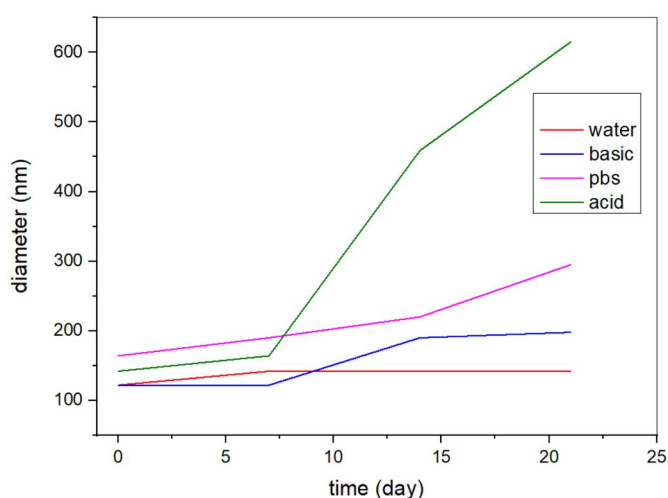


Figure 7. Stability data of $\text{Fe}_3\text{O}_4@\text{SiO}_2@\text{PDA}@\text{Ag}$ nanocomposite in water, PBS, acidic and basic buffers.

Herein, to assess the anticancer activity of $\text{Fe}_3\text{O}_4@\text{SiO}_2@\text{PDA}$ and $\text{Fe}_3\text{O}_4@\text{SiO}_2@\text{PDA}@\text{Ag}$ nanocomposite in non-small cell lung cancer cell line H1299, each cell line was treated with $\text{Fe}_3\text{O}_4@\text{SiO}_2@\text{PDA}$ and $\text{Fe}_3\text{O}_4@\text{SiO}_2@\text{PDA}@\text{Ag}$ nanocomposite with different concentration—5, 10, 20, 40, 60, 80, 100 $\mu\text{g}/\text{mL}$ for 48 h. The % viability was calculated and plotted using the spectrophotometric data for each concentration along with standard deviation (Figure 8). The graphs depict a concentration-dependent effect of $\text{Fe}_3\text{O}_4@\text{SiO}_2@\text{PDA}$ and $\text{Fe}_3\text{O}_4@\text{SiO}_2@\text{PDA}@\text{Ag}$ nanocomposite on H1299 cells lines. The IC_{50} for H1299 were calculated as 62.84 $\mu\text{g}/\text{mL}$ for $\text{Fe}_3\text{O}_4@\text{SiO}_2@\text{PDA}$. However, the IC_{50} for $\text{Fe}_3\text{O}_4@\text{SiO}_2@\text{PDA}@\text{Ag}$ nanocomposites were calculated as 21.52 $\mu\text{g}/\text{mL}$. Figure 9 displayed the microscopic images of the effect of the $\text{Fe}_3\text{O}_4@\text{SiO}_2@\text{PDA}@\text{Ag}$ nanoparticles on H1299 cancer cell line. A large population of nanoparticles (black dots) are internalised by target H1299 cancer cells.

5.3.2. Apoptosis assay of $\text{Fe}_3\text{O}_4@\text{SiO}_2@\text{PDA}@\text{Ag}$ nanoparticles using Flow cytometry

The mechanism of cell death that occurs in H1299 cells upon treatment with $\text{Fe}_3\text{O}_4@\text{SiO}_2@\text{PDA}@\text{Ag}$ nanoparticles using Annexin-V FITC/PI dual staining assay was performed, and cells were analysed using FACS. After treatment with increasing concentration for 48 h the apoptosis index in H1299 cells was increased to 21% in early apoptosis & 46 % in late apoptosis at 30 $\mu\text{g}/\text{mL}$ (Figure 10).

5.3.2. Evaluation of antibacterial activity of nanoparticles

To comprehend the potency of the $\text{Fe}_3\text{O}_4@\text{SiO}_2@\text{PDA}@\text{Ag}$ nanocomposites as antibacterial agents, we performed the standard microbroth dilution assay with both Gram-positive and Gram-negative bacteria. The results showed that the nanoparticles were effective in inhibiting the growth of these bacteria at a concentration of 115 $\mu\text{g}/\text{mL}$, for both *S. aureus* and *P. aeruginosa*, indicating another beneficial property of these nanocomposites. This activity could be attributed to the interaction of the nano-sized particles with the larger surface area of the microorganisms. The relative survival percentage of these bacteria is endorsed in Figure 11 as compared to growth controls. It is evident from the findings that the antibacterial propensity of the nanocomposite (due to 11.15 wt% of silver atom) against both Gram-positive or Gram-negative is concentration-dependent. The presence of thick peptidoglycan layer around Gram-positive bacterial cells leads to less suppression in bacterial growth at the same concentration for *S. aureus* as compared to *P. aeruginosa*.

Additionally, the SEM images displayed in Figure 12 demonstrated morphologically induced changes like rupture of the cell membrane, cell shrinkage, aggregation of bacterial cells in $\text{Fe}_3\text{O}_4@\text{SiO}_2@\text{PDA}@\text{Ag}$ nanocomposites treated samples, whereas in control cells displayed normal, smooth and well-preserved cell membrane. The nanocomposite

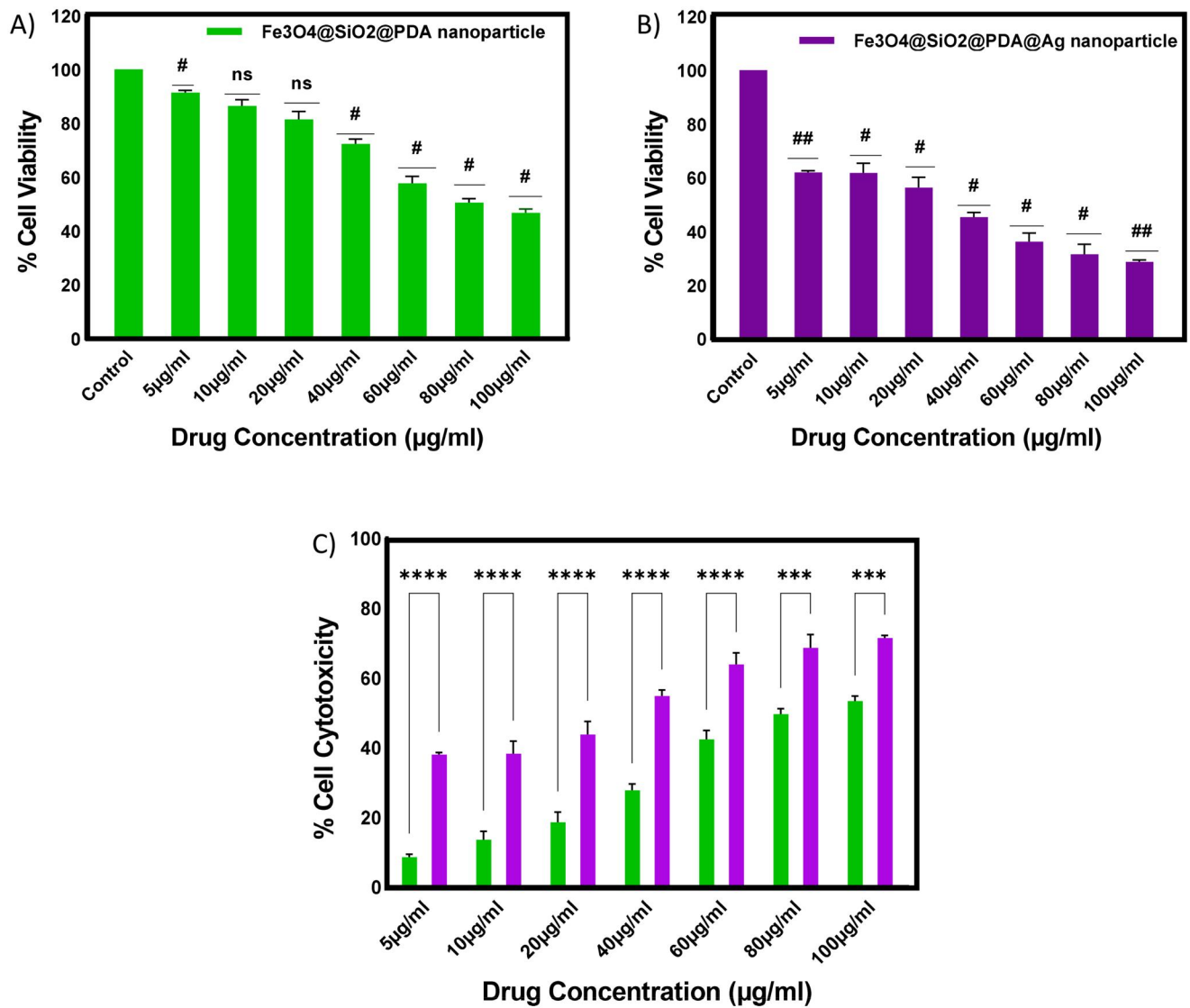


Figure 8. MTT assay at various concentrations on H1299 cancer cell line; (A) % cell viability of Fe₃O₄@SiO₂@PDA (B) % cell viability of Fe₃O₄@SiO₂@PDA@Ag (C) comparison of % cell cytotoxicity of Fe₃O₄@SiO₂@PDA and Fe₃O₄@SiO₂@PDA@Ag.

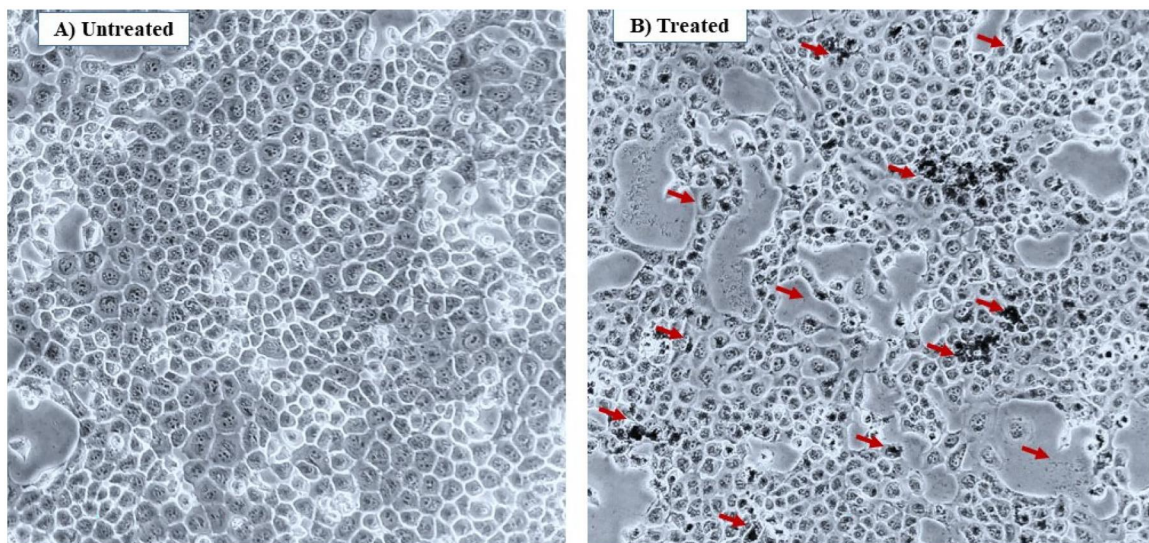


Figure 9. Microscopic images of the effect of the Fe₃O₄@SiO₂@PDA@Ag nanoparticles on H1299 cancer cell line. (A) Untreated/control (B) at 50 μg/mL.

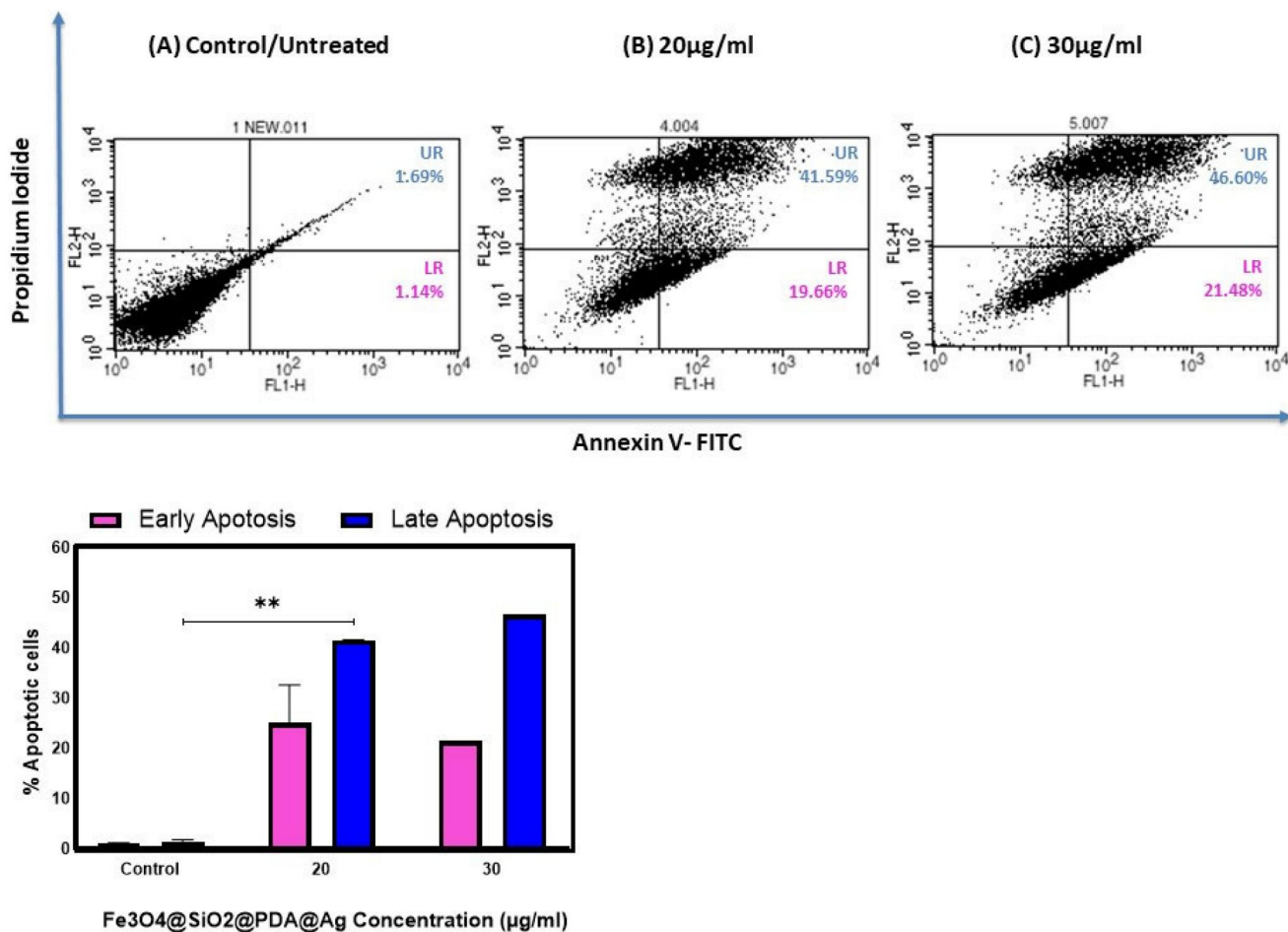


Figure 10. Cell apoptosis assay at different concentrations of $\text{Fe}_3\text{O}_4@\text{SiO}_2@\text{PDA}@Ag$ on H1299 cancer cell line (A) control; 0 $\mu\text{g/ml}$, (B) 20 $\mu\text{g/ml}$, (C) 30 $\mu\text{g/ml}$.

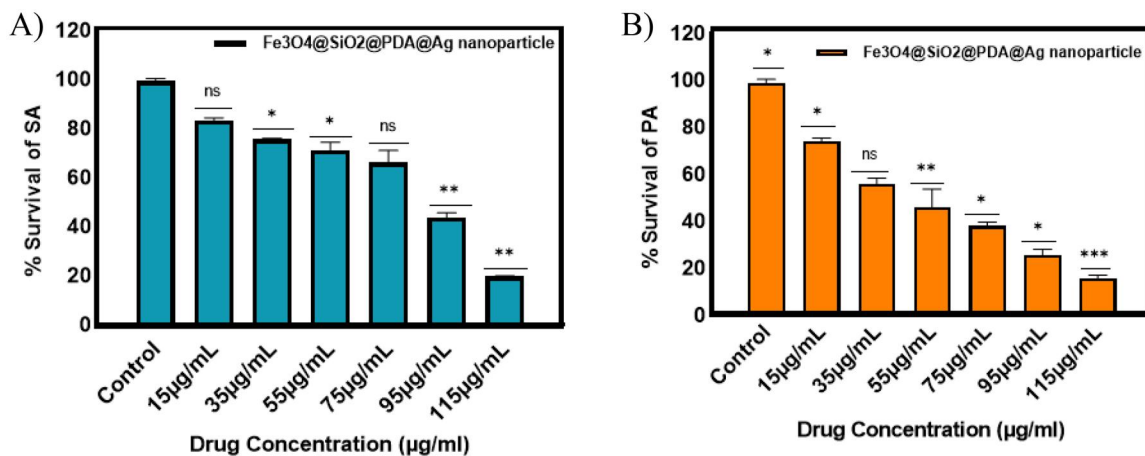


Figure 11. Antibacterial activity of $\text{Fe}_3\text{O}_4@\text{SiO}_2@\text{PDA}@Ag$ nanocomposites with increasing concentrations against (A) *S. aureus* and (B) *P. aeruginosa*.

treated cell had deformed and distorted cell structure indicating leakage of intracellular components. SEM images clearly indicated morphological alterations along with complete lysis of the outer membrane of bacteria. EDX analysis also confirmed the presence of strong Ag metallic signals in treated cells. Other signals like Si and Fe were observed due to the $\text{Fe}_3\text{O}_4@\text{SiO}_2$ shell present in the nanocomposite, in addition to the C, N, O present attributed to the bacterial biomolecules.

5.4. In vitro Haemolysis assay

Haemolysis study was conducted with 100, 250, 350, 450, 550 and 650 $\mu\text{g/ml}$ concentrations of $\text{Fe}_3\text{O}_4@\text{SiO}_2@\text{PDA}@Ag$ nanoparticles. The haemolysis was found to be minimal at a concentration of 100 $\mu\text{g/ml}$. This concentration is relatively higher than the observed IC_{50} value (21.52 $\mu\text{g/ml}$) for this nanocomposite. At maximum concentration (650 $\mu\text{g/ml}$), which was 30 times the observed IC_{50} , the haemolysis was negligible. These

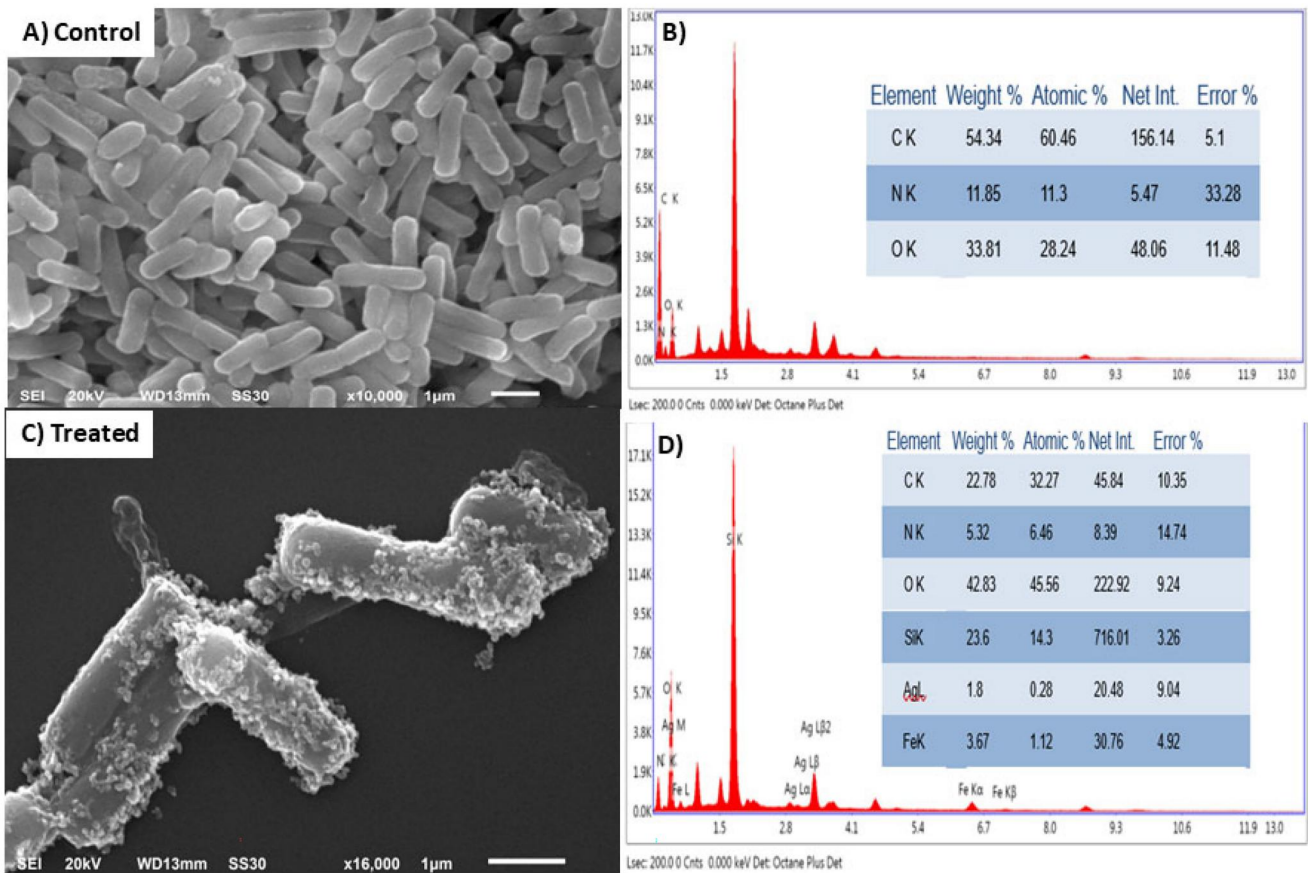


Figure 12. Scanning electron micrographs of (A) and (B) untreated *P. aeruginosa* cells and its EDAX composition (C) and (D) cells treated with $Fe_3O_4@SiO_2@PDA@Ag$ nanocomposites at MIC and its EDAX composition.

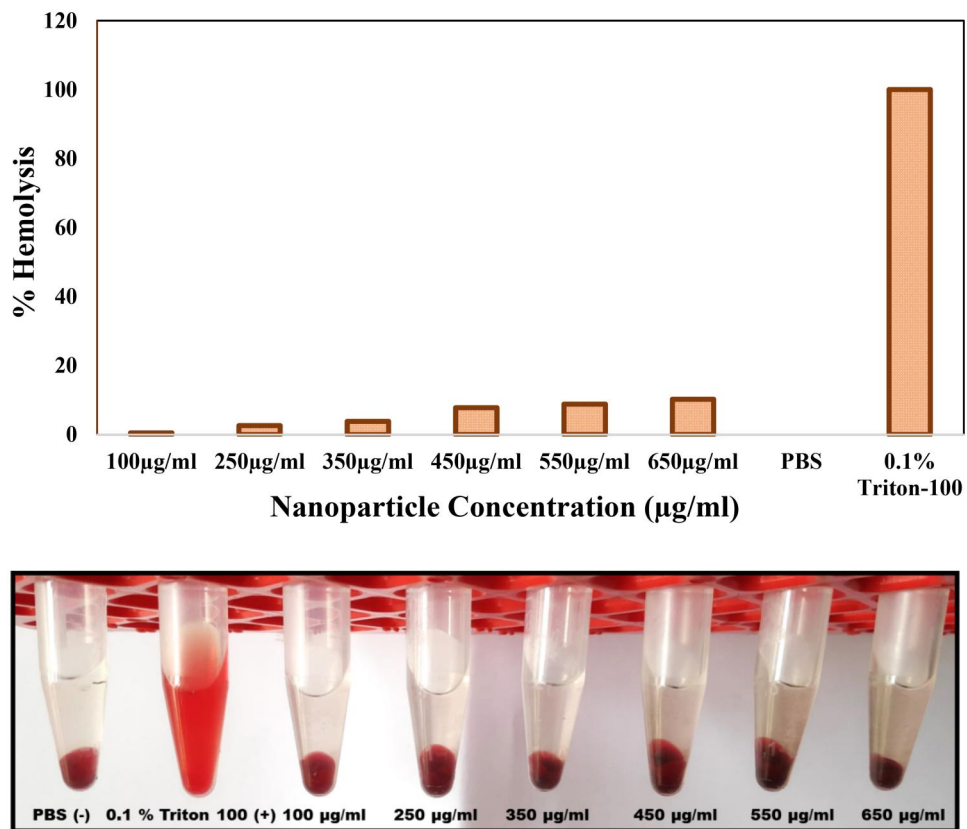


Figure 13. Haemolysis assay of $Fe_3O_4@SiO_2@PDA@Ag$ nanoparticle at various concentrations.

observations demonstrated that these nanoparticles can be used directly or can be used as a drug delivery agent, which can reduce their toxicity on human cells (Figure 13).

6. Conclusion

Lung cancer is the most aggressive human cancer and a leading cause of death worldwide. Here, we have reported a simple protocol to synthesise Ag-wrapped $\text{Fe}_3\text{O}_4@\text{SiO}_2@\text{PDA}$ nanocomposites. The anticancer and antibacterial activity displayed by the Ag nanocomposites reported here represent a better alternative to available options. We have also shown the mode of cell death using apoptosis assay and biocompatibility of synthesised nanocomposites using haemolysis assay. The nanocomposites have effusively demonstrated their antibacterial activity against Gram-positive and Gram-negative bacteria but with different susceptibilities at the same concentration range. Thus, the ordinance of these nanocomposites serves as a lucrative option in this ever-evolving era of bacterial infections.

Acknowledgements

Prof. Ramesh Chandra would like to acknowledge University of Delhi for providing support and necessary facilities to carry out research work. Snigdha Singh is grateful to DST (Indo-Russia: INT/RUS/RFBR/389) for providing the financial assistance. Tanya Goel is thankful to DST-Inspire Fellowship for their assistance. Heerak Chugh and Aarushi Singh are thankful to ICMR for providing Senior Research Fellowship.

Disclosure statement of interest

The authors declare no potential competing interest.

Funding

R.C. and S.S. are grateful to DST (Indo-Russia: INT/RUS/RFBR/389) for providing the financial assistance. R.C. and A.S. are grateful to ICMR-SRF (45/10/2020-Nan/BMS) for providing the fellowship.

ORCID

Snigdha Singh  <http://orcid.org/0000-0003-0319-8887>
Ramesh Chandra  <http://orcid.org/0000-0002-3040-997X>

Data availability statement

Raw data available on request.

Author's contribution

R.C., S.S., and T.G. contributed to the idea or design of the work. S.S., A.S., T.G. and H.C. performed the nanoparticle synthesis, characterization, analysis and interpretation of data for the work. H.C. and T.G. performed the anticancer activity and did the interpretation of the results. T.G. and M.T. did the apoptosis experiment and analysed the data. N.C. and I.R. did the antibacterial experiments and analysed the data. R.C., S.S. and M.T. supervised the project. S.S., A.S., T.G., H.C., N.C., I.R., M.T. and R.C. contributed to the drafting of the work, reviewing the intellectual content of the manuscript. All authors have agreed to the final version, helped in analysis of the data and provided critical feedbacks during the writing and revision of the manuscript.

References

- [1] Ferlay J, Colombet M, Soerjomataram I, et al. Cancer statistics for the year 2020: an overview. *Int J Cancer*. 2021;149(4):778–789. doi: [10.1002/ijc.33588](https://doi.org/10.1002/ijc.33588).
- [2] Esteban EC, Rullán JAD, Castillo PB, et al. Current role of nanoparticles in the treatment of lung cancer. *Campos J Clin Transl Sci*. 2021;7:140–155.
- [3] Baig N, Kammakam I, Falath W. Nanomaterials: a review of synthesis methods, properties, recent progress, and challenges. *Mater Adv*. 2021;2(6):1821–1871. doi: [10.1039/D0MA00807A](https://doi.org/10.1039/D0MA00807A).
- [4] Dabagh S, Haris SA, Isfahani BK, et al. Silver-decorated and silica-capped magnetite nanoparticles with effective antibacterial activity and reusability. *ACS Appl Bio Mater*. 2023;6(6):2266–2276. doi: [10.1021/acsabm.3c00122](https://doi.org/10.1021/acsabm.3c00122).
- [5] Pei J, Fu B, Jiang L, et al. Biosynthesis, characterization, and anticancer effect of plant-mediated silver nanoparticles using *Coptis chinensis*. *Int J Nanomed*. 2019;14:1969–1978. doi: [10.2147/IJN.S188235](https://doi.org/10.2147/IJN.S188235).
- [6] Romdoni Y, Kadja GTM, Kitamoto Y, et al. Synthesis of multifunctional $\text{Fe}_3\text{O}_4@\text{SiO}_2\text{-Ag}$ nanocomposite for antibacterial and anticancer drug delivery. *Appl Surf Sci*. 2022;610:155610. doi: [10.1016/j.apsusc.2022.155610](https://doi.org/10.1016/j.apsusc.2022.155610).
- [7] Austin LA, Mackey MA, Dreaden EC, et al. The optical, photothermal, and facile surface chemical properties of gold and silver nanoparticles in biodiagnostics, therapy, and drug delivery. *Arch Toxicol*. 2014;88(7):1391–1417. doi: [10.1007/s00204-014-1245-3](https://doi.org/10.1007/s00204-014-1245-3).
- [8] Mohanta YK, Biswas K, Panda SK, et al. Phyto-assisted synthesis of bio-functionalised silver nanoparticles and their potential anti-oxidant, anti-microbial and wound healing activities. *IET Nanobiotechnol*. 2017;11(8):1027–1034. doi: [10.1049/iet-nbt.2017.0017](https://doi.org/10.1049/iet-nbt.2017.0017).
- [9] Zahran M, Khalifa Z, Zahran MA-H, et al. Recent advances in silver nanoparticle-based electrochemical sensors for determining organic pollutants in water: a review. *Mater Adv*. 2021;2(22):7350–7365. doi: [10.1039/D1MA00769F](https://doi.org/10.1039/D1MA00769F).
- [10] Wang ZX, Chen CY, Wang Y, et al. Ångstrom-scale silver particles as a promising agent for low-toxicity broad-spectrum potent anticancer therapy. *Adv Funct Mater*. 2019;29:1808556.
- [11] Stensberg MC, Wei Q, McLamore ES, et al. Toxicological studies on silver nanoparticles: challenges and opportunities in assessment, monitoring and imaging. *Nanomedicine (Lond)*. 2011;6(5):879–898. doi: [10.2217/nnm.11.78](https://doi.org/10.2217/nnm.11.78).
- [12] Algotiml R, Gab-Alla A, Seoudi R, et al. Anticancer and antimicrobial activity of biosynthesized Red Sea marine algal silver nanoparticles. *Sci Rep*. 2022;12(1):2421. doi: [10.1038/s41598-022-06412-3](https://doi.org/10.1038/s41598-022-06412-3).
- [13] Liu L, Wang M, Liu C, et al. Effective gene delivery based on facilely synthesized “core-shell” $\text{Ag}@PDA@PEI$ nanoparticles. *J Nanopart Res*. 2022;24(9):184. doi: [10.1007/s11051-022-05571-8](https://doi.org/10.1007/s11051-022-05571-8).
- [14] Pieretti JC, Rolim WR, Ferreira FF, et al. Synthesis, characterization, and cytotoxicity of $\text{Fe}_3\text{O}_4@\text{Ag}$ hybrid nanoparticles: promising applications in cancer treatment. *J Clust Sci*. 2020;31(2):535–547. doi: [10.1007/s10876-019-01670-0](https://doi.org/10.1007/s10876-019-01670-0).
- [15] He Y, Du Z, Ma S, et al. Effects of green-synthesized silver nanoparticles on lung cancer cells in vitro and grown as xenograft tumors in vivo. *Int J Nanomedicine*. 2016;11:1879–1887. doi: [10.2147/IJN.S103695](https://doi.org/10.2147/IJN.S103695).
- [16] Gengan RM, Anand K, Phulukdaree A, et al. A549 lung cell line activity of biosynthesized silver nanoparticles using *Albizia adianthifolia* leaf. *Colloids Surf B Biointerf*. 2013;105:87–91. doi: [10.1016/j.colsurfb.2012.12.044](https://doi.org/10.1016/j.colsurfb.2012.12.044).
- [17] Silva AC, Oliveira TR, Mamani JB, et al. Application of hyperthermia induced by superparamagnetic iron oxide nanoparticles in glioma treatment. *Int J Nanomed*. 2011;6:591–603. doi: [10.2147/IJN.S14737](https://doi.org/10.2147/IJN.S14737).
- [18] Tian S, Saravanan K, Mothana RA, et al. Anti-cancer activity of biosynthesized silver nanoparticles using *avicennia marina* against A549 lung cancer cells through ROS/mitochondrial damages.

- Saudi J Biol Sci. 2020;27(11):3018–3024. doi: [10.1016/j.sjbs.2020.08.029](https://doi.org/10.1016/j.sjbs.2020.08.029).
- [19] Jeyaraj M, Rajesh M, Arun R, et al. An investigation on the cytotoxicity and caspase-3-mediated apoptotic effect of biologically synthesized silver nanoparticles using podophyllum hexandrum on human cervical carcinoma cells. *Colloids Surf B Biointerf.* 2013; 102:708–717. doi: [10.1016/j.colsurfb.2012.09.042](https://doi.org/10.1016/j.colsurfb.2012.09.042).
- [20] Rashidipour M, Heydari R. Biosynthesis of silver nanoparticles using extract of olive leaf: synthesis and in vitro cytotoxic effect on MCF-7 cells. *J Nanostructure Chem.* 2014;4:112.
- [21] Heydari R, Rashidipour M. Green synthesis of silver nanoparticles using extract of oak fruit hull (jaft): synthesis and in vitro cytotoxic effect on MCF-7 cells. *Int J Breast Cancer.* 2015;2015: 846743–846746. doi: [10.1155/2015/846743](https://doi.org/10.1155/2015/846743).
- [22] Sangour MH, Ali IM, Atwan ZW, et al. Effect of Ag nanoparticles on viability of MCF-7 and vero cell lines and gene expression of apoptotic genes. *Egypt J Med Hum Genet.* 2021;22(1):9. doi: [10.1186/s43042-020-00120-1](https://doi.org/10.1186/s43042-020-00120-1).
- [23] Miyazawa N, Hakamada M, Mabuchi M. Antimicrobial mechanisms due to hyperpolarisation induced by nanoporous Au. *Sci Rep.* 2018;8(1):3870. doi: [10.1038/s41598-018-22261-5](https://doi.org/10.1038/s41598-018-22261-5).
- [24] Wang L, Hu C, Shao L. The antimicrobial activity of nanoparticles: present situation and prospects for the future. *Int J Nanomed.* 2017;12:1227–1249. doi: [10.2147/IJN.S121956](https://doi.org/10.2147/IJN.S121956).
- [25] Quirós J, Borges JP, Boltes K, et al. Antimicrobial electrospun silver-, copper- and zinc-doped polyvinylpyrrolidone nanofibers. *J Hazard Mater.* 2015;299:298–305. doi: [10.1016/j.jhazmat.2015.06.028](https://doi.org/10.1016/j.jhazmat.2015.06.028).
- [26] Heydari R, Koudehi MF, Pourmortazavi SM. Antibacterial activity of Fe₃O₄/Cu nanocomposite: green synthesis using *Carum carvi* L. Seeds Aqueous Extract. *Chemistry Select.* 2019.
- [27] Bezza FA, Tichapondwa SM, Chirwa EMN. Fabrication of monodispersed copper oxide nanoparticles with potential application as antimicrobial agents. *Sci Rep.* 2020;10(1):16680. doi: [10.1038/s41598-020-73497-z](https://doi.org/10.1038/s41598-020-73497-z).
- [28] Agnihotri S, Bajaj G, Mukherji S, et al. Arginine-assisted immobilization of silver nanoparticles on ZnO nanorods: an enhanced and reusable antibacterial substrate without human cell cytotoxicity. *Nanoscale.* 2015;7(16):7415–7429. doi: [10.1039/c4nr06913g](https://doi.org/10.1039/c4nr06913g).
- [29] Fekri MH, Tousi F, Heydari R, et al. Synthesis of magnetic novel hybrid nanocomposite (Fe₃O₄@SiO₂/activated carbon) by a green method and evaluation of its antibacterial potential. *Iran J Chem Chem Eng.* 2022;41:767–776.
- [30] Chi Y, Yuan Q, Li Y, et al. Synthesis of Fe₃O₄@SiO₂-Ag magnetic nanocomposite based on small-sized and highly dispersed silver nanoparticles for catalytic reduction of 4-nitrophenol. *J Colloid Interface Sci.* 2012;383(1):96–102. doi: [10.1016/j.jcis.2012.06.027](https://doi.org/10.1016/j.jcis.2012.06.027).
- [31] Pallavicini P, Taglietti A, Dacarro G, et al. Self-assembled monolayers of silver nanoparticles firmly grafted on glass surfaces: low Ag⁺ release for an efficient antibacterial activity. *J Colloid Interface Sci.* 2010;350(1):110–116. doi: [10.1016/j.jcis.2010.06.019](https://doi.org/10.1016/j.jcis.2010.06.019).
- [32] Farzad E, Veisi H. Fe₃O₄/SiO₂ nanoparticles coated with polydopamine as a novel magnetite reductant and stabilizer sorbent for palladium ions: synthetic application of Fe₃O₄/SiO₂@PDA/Pd for reduction of 4-nitrophenol and Suzuki reactions. *J Indus Eng Chem.* 2018;60:114–124. doi: [10.1016/j.jiec.2017.10.017](https://doi.org/10.1016/j.jiec.2017.10.017).
- [33] Sharma RK, Dutta S, Sharma S, et al. Fe₃O₄ (iron oxide)-supported nanocatalysts: synthesis, characterization and applications in coupling reactions. *Green Chem.* 2016;18(11):3184–3209. doi: [10.1039/C6GC00864J](https://doi.org/10.1039/C6GC00864J).
- [34] Qianjun H, Jianlin S. Mesoporous silica nanoparticle based nano drug delivery systems: synthesis, controlled drug release and delivery, pharmacokinetics and biocompatibility. *J Mater Chem.* 2011;21(16):5845–5855. doi: [10.1039/c0jm03851b](https://doi.org/10.1039/c0jm03851b).
- [35] Dolui SK, Das D, Choudhury P, et al. Synthesis and characterization of SiO₂/polyaniline/Ag core-shell particles and studies of 2 their electrical and hemolytic properties: multifunctional core-shell particles. *RSC Adv.* 2014, 5, 2360–2367.
- [36] Abbas M. Fe₃O₄/SiO₂ core/shell nanocubes: novel coating approach with tunable silica thickness and enhancement in stability and biocompatibility. *J Nanomed Nanotechnol.* 2014; 5(06), 244. doi: [10.4172/2157-7439.1000244](https://doi.org/10.4172/2157-7439.1000244).
- [37] Lee H, Dellatore SM, Miller WM, et al. Mussel-Inspired surface chemistry for multifunctional coatings. *Science.* 2007;318(5849): 426–430. doi: [10.1126/science.1147241](https://doi.org/10.1126/science.1147241).
- [38] Murari G, Bock N, Zhou H, et al. Effects of polydopamine coatings on nucleation modes of surface mineralization from simulated body fluid. *Sci Rep.* 2020;10(1):14982. doi: [10.1038/s41598-020-71900-3](https://doi.org/10.1038/s41598-020-71900-3).
- [39] Barclay TG, et al. Versatile surface modification using polydopamine and related polycatecholamines: chemistry, structure, and applications. *Adv Mater Interf.* 2017;4:1601192.
- [40] Hong SH, et al. Sprayable ultrafast polydopamine surface modifications. *Adv Mater Interf.* 2016;3:1500857.
- [41] Ryu JH, Messersmith PB, Lee H. Polydopamine surface chemistry: a decade of discovery. *ACS Appl Mater Interf.* 2018;10(9):7523–7540. doi: [10.1021/acsami.7b19865](https://doi.org/10.1021/acsami.7b19865).
- [42] Baskoutas S. Solid-state synthesis of Ag-doped PANI nanocomposites for their end-use as an electrochemical sensor for hydrogen peroxide and dopamine. *Electrochim Acta.* 2020, 363, 137158.
- [43] Zhang N, Peng S, Liu Z, et al. Ag NPs decorated on the magnetic Fe₃O₄@PDA as efficient catalyst for organic pollutants removal and as effective antimicrobial agent for microbial inhibition. *J Alloys Compd.* 2022;928:167257. doi: [10.1016/j.jallcom.2022.167257](https://doi.org/10.1016/j.jallcom.2022.167257).
- [44] Wang G, Yang F, Huang W, et al. Recyclable Mussel-Inspired magnetic nanocellulose@polydopamine-Ag nanocatalyst for efficient degradation of refractory organic pollutants and bacterial disinfection. *ACS Appl Mater Interf.* 2022;14(46):52359–52369. doi: [10.1021/acsami.2c13915](https://doi.org/10.1021/acsami.2c13915).
- [45] Nikmah A, Taufiq A, Hidayat A, et al. Excellent antimicrobial activity of Fe₃O₄/SiO₂/Ag nanocomposites. *NANO Brief Rep Rev.* 2021; 16:2150049. doi: [10.1142/S1793292021500491](https://doi.org/10.1142/S1793292021500491).
- [46] Lv B, Xu Y, Tian H, et al. Synthesis of Fe₃O₄/SiO₂ nanoparticles and its application in surface-enhanced Raman scattering. *J Solid State Chem.* 2010;183(12):2968–2973. doi: [10.1016/j.jssc.2010.10.001](https://doi.org/10.1016/j.jssc.2010.10.001).
- [47] Sun M, Zhao A, Wang D, et al. Cube-like Fe₃O₄@SiO₂@Au@Ag magnetic nanoparticles: a highly efficient SERS substrate for detection of pesticide. *Nanotechnology.* 2018;29(16):165302. doi: [10.1088/1361-6528/aaae42](https://doi.org/10.1088/1361-6528/aaae42).
- [48] Gupta R, Yadav M, Gaur R, et al. A straightforward one-pot synthesis of bioactive N-aryl oxazolidin-2-ones via a highly efficient Fe₃O₄/SiO₂-supported acetate-based butylimidazolium ionic liquid nanocatalyst under metal- and solvent-free conditions. *Green Chem.* 2017;19(16):3801–3812. doi: [10.1039/C7GC01414G](https://doi.org/10.1039/C7GC01414G).
- [49] Yu X, Cheng G, Zheng SY. Synthesis of self-assembled multifunctional nanocomposite catalysts with highly stabilized reactivity and magnetic recyclability. *Sci Rep.* 2016;6:25459. doi: [10.1038/srep25459](https://doi.org/10.1038/srep25459).
- [50] Liaqat N, Jahan N, Anwar T, et al. Green synthesized silver nanoparticles: optimization, characterization, antimicrobial activity, and cytotoxicity study by hemolysis assay. *Front Chem.* 2022;10: 952006. doi: [10.3389/fchem.2022.952006](https://doi.org/10.3389/fchem.2022.952006).
- [51] Yadav S, Deka SR, Verma G, et al. Photoresponsive amphiphilic-zobenzene-PEG self-assembles to form supramolecular nanostructures for drug delivery applications. *RSC Adv.* 2016;6(10):8103–8117. doi: [10.1039/C5RA26658K](https://doi.org/10.1039/C5RA26658K).
- [52] Shivhare K, Garg C, Priyam A, et al. Enzyme sensitive smart inulin-dehydropeptide conjugate self-assembles into nanostructures useful for targeted delivery of ornidazole. *Int J Biol Macromol.* 2018;106:775–783. doi: [10.1016/j.jbiomac.2017.08.071](https://doi.org/10.1016/j.jbiomac.2017.08.071).
- [53] Fuentes-García JA, Diaz-Cano AI, Guillen-Cervantes A, et al. Magnetic domain interactions of Fe₃O₄ nanoparticles embedded in a SiO₂ matrix. 2018;8:5096.
- [54] Kalishwaralal K, Deepak V, Ramkumarandian S, et al. Extracellular biosynthesis of silver nanoparticles by the culture supernatant of *Bacillus licheniformis*. *Mater Lett.* 2008;62(29):4411–4413. doi: [10.1016/j.matlet.2008.06.051](https://doi.org/10.1016/j.matlet.2008.06.051).